HTML ABSTRACT * LINKS

Bright green electroluminescence from Tb^{3+} in silicon metal-oxide-semiconductor devices

J. M. Sun,[a] W. Skorupa, T. Dekorsy,[b] and M. Helm
Institute of Ion Beam Physics and Materials Research, Forschungszentrum Rossendorf, P.O. Box 510119, D-01314 Dresden, Germany

L. Rebohle and T. Gebel
Nanoparc Gesellschaft mit Beschränkter Haftung (GmbH), D-01454 Dresden, Germany

(Received 11 February 2005; accepted 27 April 2005; published online 20 June 2005)

Bright green electroluminescence with luminance up to 2800 cd/m^2 is reported from indium-tin-oxide/SiO_2:Tb/Si metal-oxide-semiconductor devices. The SiO_2:Tb^{3+} gate oxide was prepared by thermal oxidation followed by Tb^+ implantation. Electroluminescence and photoluminescence properties were studied with variations of the Tb^{3+} ion concentration and the annealing temperature. The optimized device shows a high external quantum efficiency of 16% and a luminous efficiency of 2.1 lm/W. The excitation processes of the strong green electroluminescence are attributed to the impact excitation of the Tb^{3+} luminescent centers by hot electrons and the subsequent crossrelaxation from $^5D_3$ to $^5D_4$ energy levels. Light-emitting devices with micrometer size fabricated by the standard metal-oxide-semiconductor technology are demonstrated. © *2005 American Institute of Physics*. [DOI: 10.1063/1.1935766]

I. INTRODUCTION

The combination of silicon-based electronic circuits with optoelectronic functionality is one of the key challenges for future semiconductor technology.[1] As the packaging density of transistors becomes higher and higher in ultralarge-scale integrated (ULSI) circuits, the problems of overheating and signal delay become serious due to the drastic increase of metallic connects. One possible solution could be optical interconnects integrated with silicon technology.[2] The implementation of silicon-based optical interconnections requires light emitters, waveguides, modulators, and photodetectors.[3] Since bulk silicon is an inherently bad light emitter for its indirect electronic band structure, hybrid systems with III-V photonic components have to be used until an efficient, reliable silicon-based light source becomes available.[4]

Recently, several approaches for gaining light from silicon-based systems have been reported with the prospect of sufficient electroluminescence (EL) efficiency. The most prominent systems are porous silicon,[5] silicon nanocrystals in SiO_2,[6] *p-n* diodes,[7,8] Ge^+-implanted SiO_2,[9] and Er-doped silicon-rich SiO_2 sensitized with silicon nanocrystals.[10,11] The latter ones, realized as metal-oxide-semiconductor (MOS) light emitters, are especially attractive, since they are fully compatible with silicon complementary metal-oxide-semiconductor (CMOS) technology. Efficient MOS EL devices have been fabricated by erbium-doped silicon-rich SiO_2 with the attractive infrared light emission at 1.54 μm for telecommunications.[12]

Another driving force for developing silicon-based light emitters is the requirement of tiny light sources in the visible and ultraviolet regions, which can be directly integrated into silicon chips for analysis of different biological substances, for silicon optical couplers, and high-resolution low-cost microdisplays. Rare-earth-doped silicon MOS light emitters with different emission wavelengths from the visible up to ultraviolet are feasible for these applications. Photoluminescence (PL) from rare-earth-doped SiO_2 thin films on silicon has been studied extensively in the past, such as Si-rich SiO_2:Tm^{3+} (Ref. 13) and SiO_2:Tb^{3+}.[14,15] However, *electroluminescence* from rare-earth-doped MOS structures has not been studied much due to the limited current injection into the dielectric SiO_2 layer and the poor reliability at high electric field (charge to breakdown). One solution for this problem is the introduction of excess silicon into SiO_2. The rare-earth-doped Si-rich SiO_2 thin films have exhibited an improved stability under high-density current injection; however, it comes at the expense of a lower EL efficiency compared to stoichiometric SiO_2 due to an increase of low-energy electron tunneling between the silicon clusters. Recently we have reported an efficient and stable electroluminescent Gd-doped MOS device, emitting deep UV light with an external quantum efficiency above 1%.[16] In this paper, efficient green EL from Tb-implanted SiO_2 MOS devices is reported with a maximum luminance above 2800 cd/m^2. The maximum external quantum efficiency is 16% with a luminous efficiency above 2.1 lm/W. The EL and PL properties of the Tb-doped SiO_2 active layers are studied concerning variations of the Tb concentration and the annealing temperature. The excitation process of the EL from Tb^{3+} in the SiO_2 matrix is also discussed based on the study of the photoluminescence excitation spectra, the intensity ratio of the blue to green peak (B/G ratio), the luminescence decay time, and the crossrelaxation.

[a]Author to whom correspondence should be addressed; electronic mail: j.sun@fz-rossendorf.de
[b]Present address: Fachbereich Physik, Universität Konstanz, 78457 Konstanz, Germany.

0021-8979/2005/97(12)/123513/7/$22.50 © 2005 American Institute of Physics

Downloaded 21 Jun 2005 to 134.34.145.184. Redistribution subject to AIP license or copyright, see http://jap.aip.org/jap/copyright.jsp

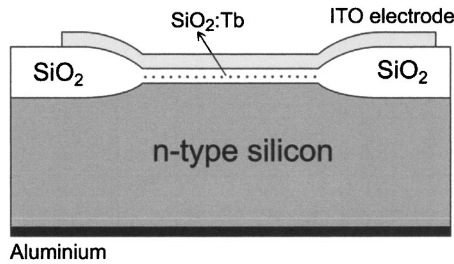

FIG. 1. Schematic structure of the $SiO_2:Tb^{3+}$ MOS light-emitting device.

II. EXPERIMENTAL METHODS

Samples were prepared by silicon metal-oxide-semiconductor technology on a 4-in. {100}-oriented *n*-type silicon wafer with resistivity of 2–5 Ω cm. The MOS structures were fabricated by local oxidation of silicon (LOCOS) with gate oxide and a field oxide thickness of 1 μm, as shown in the diagram of Fig. 1. The active layer in the gate oxide is a 100-nm-thick thermally grown SiO_2 implanted with Tb^+ ions at two energies of 50 and 110 keV. The implantation doses were adjusted to generate a nearly constant Tb concentration in the depth range of 27–55 nm below the surface of the active layer. Figure 2 shows the profiles of the as-implanted Tb atoms in the SiO_2 layer with a concentration of 1.5%. The Tb profiles were calculated by TRIM98 as a first estimation, and confirmed by Rutherford backscattering spectrometry (RBS). The Tb atomic concentration was varied from 0.05% to 3% for different samples. The implantation was followed by furnace annealing at 800–1100 °C in flowing N_2 for 1 h. The gate electrode is a 100-nm transparent indium-tin-oxide layer deposited by rf sputtering. Various shapes of MOS devices with different feature sizes in the range from 2 to 500 μm were fabricated for testing the operation of the EL devices in dependence on the geometry.

EL spectra were measured on a MOS structure with a circular indium tin oxide (ITO) electrode of 500-μm diameter at a constant current supplied by a source meter (Keithley 2410). EL is observed at both positive and negative polarities of the applied voltage. The measurement was normally done with electron injection from the silicon substrate to the Tb-doped SiO_2. The EL signal was recorded at room temperature with a monochromator (Jobin Yvon Triax 320)

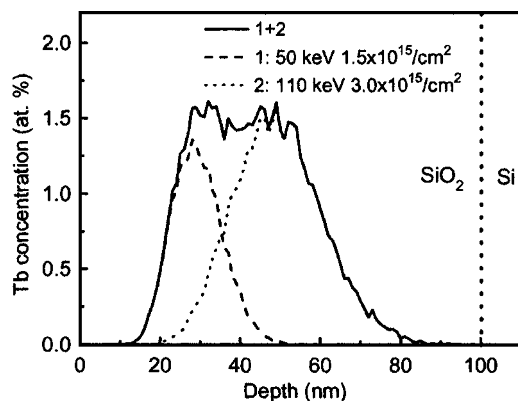

FIG. 2. Profiles of the implanted Tb atoms at double energies of 50 and 110 keV calculated by TRIM98. The Tb^+ doses are 1.5×10^{15} and $3.0\times10^{15}/cm^2$, respectively, for a Tb concentration of 1.5%.

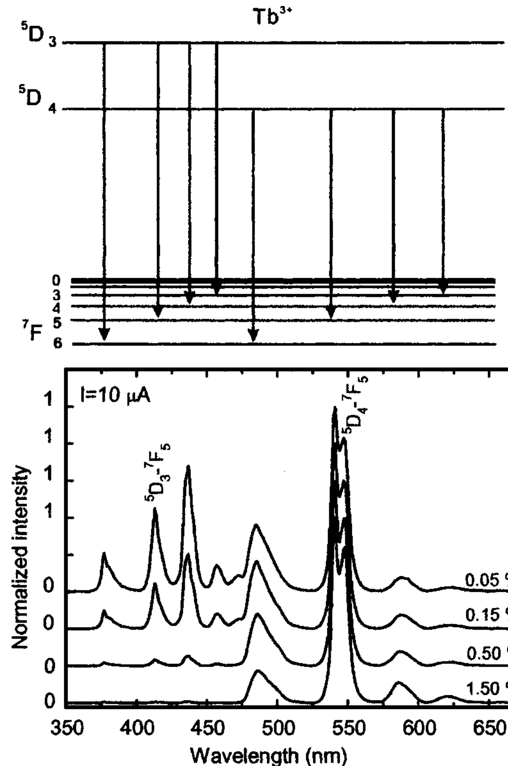

FIG. 3. EL spectra of Tb^{3+} ions in MOS devices with different Tb concentrations and the related electronic transitions. All spectra are measured at a constant injection current of 10 μA and are normalized according to the peak intensity of the $^5D_4-^7F_5$ transitions at 541 nm.

and a photomultiplier (Hamamatsu H7732-10). The EL intensity, the injection current, and the applied voltage were recorded simultaneously with a multiple channel data acquisition system. The absolute EL power from the device was measured using a calibrated optical power meter (Newport 818-SL). The external EL power efficiency was calculated by integrating the total EL output power from the front surface of the devices and by dividing the total electric input power. PL and PL excitation (PLE) spectra were also measured with the same system using a 75-W xenon lamp as an ultraviolet light source. The decay time of EL was measured by a multichannel scaler (Stanford Research System SR430, minimum time resolution of 10 ns) under the excitation of 100 -μs voltage pulses.

III. RESULTS AND DISCUSSION

A. EL and current-field characteristics

Figure 3 shows the electronic transitions and the EL spectra of different MOS devices with a 100-nm $SiO_2:Tb^{3+}$ active layer containing different Tb concentrations of 0.05%, 0.15%, 0.5%, and 1.5%. The spectra are normalized to the same amplitude of the green EL peak at 541 nm. All samples were annealed at 800 °C for 1 h. The spectra exhibit two groups of peaks, from $^5D_3$ and $^5D_4$, respectively, to ^7F_j ($j=3-6$) levels of the Tb^{3+} ions,[17] as sketched in the diagram of Fig. 3. The relative intensity of the $^5D_3-^7F_j$ (j=3–6) transitions decreases with increasing Tb^{3+} concentration, which is not the case for the $^5D_4-^7F_j$ transitions. Figure 4(a) shows the current–electric-field characteristics for devices

Downloaded 21 Jun 2005 to 134.34.145.184. Redistribution subject to AIP license or copyright, see http://jap.aip.org/jap/copyright.jsp

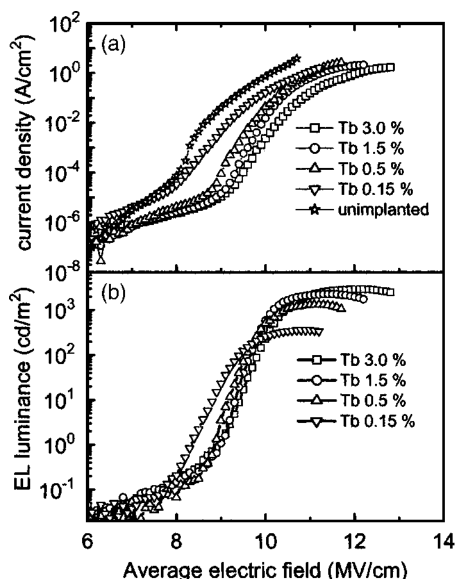

FIG. 4. (a): Current-density vs electric-field (J–E) characteristics for samples with different Tb concentrations of 0.15%, 0.5%, 1.5%, and 3%. The unimplanted thermally grown SiO_2 sample is also shown for comparison. (b): Dependence of the EL luminance on the average electric field for the same Tb-doped samples.

with different Tb concentrations of 0.15%, 0.5%, 1.5%, and 3%. The current-field characteristic of the unimplanted SiO_2 is also shown for comparison. At a low average electric field below 8 MV/cm, the small injection current results mainly from the tunneling of electrons between the residual defects in the oxide layer. An onset of strong current injection regime is observed upon increasing the electric field above 8–9 MV/cm. The strong current injection is verified as Fowler–Nordheim (FN) tunneling injection of electrons at the Si/SiO_2 interface, as shown in Fig. 5. The FN tunneling is expressed as $J/E^2 = A\exp(-B/E)$, where J is the current density, E is the average electric field, and A and B are constants.[18] From the linear fit of $\log(J/E^2)$ versus the reciprocal electric field in Fig. 5, the FN tunneling expression for the Tb-implanted SiO_2 layers is valid over a large range of J/E^2 from 1×10^{-7} to 1×10^{-3} A/(MV)^2. The current-field characteristics turn to a linear regime at higher current due to the series resistance of the device structure. The threshold electric field for the FN tunneling slightly shifts from 8 to 9 MV/cm with increasing Tb concentration. This is probably caused by a shift of the flatband voltage of the MOS device due to an increase of electron traps, as deduced from the capacitance–voltage (C–V) characteristics. Figure 4(b) shows the dependence of the EL brightness of the green peak at 541 nm on the average electric field for devices with different Tb concentrations. The onset of the EL emission is correlated with the strong current injection by FN tunneling. This indicates that the excitation of EL from Tb^{3+} ions is due to a strong FN tunneling injection of hot electrons from the silicon substrate to the conduction band of SiO_2.

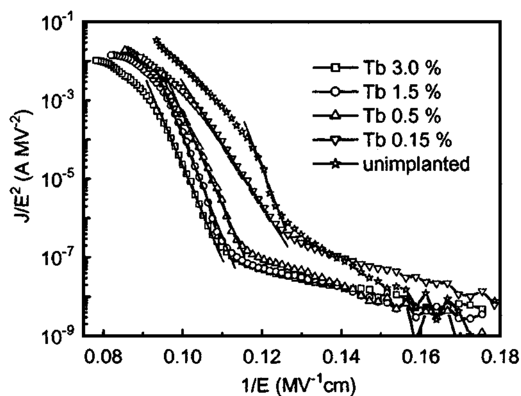

FIG. 5. Fowler–Nordheim plots of the logarithmic J/E^2 vs the reciprocal of the electric field for samples with different Tb concentrations.

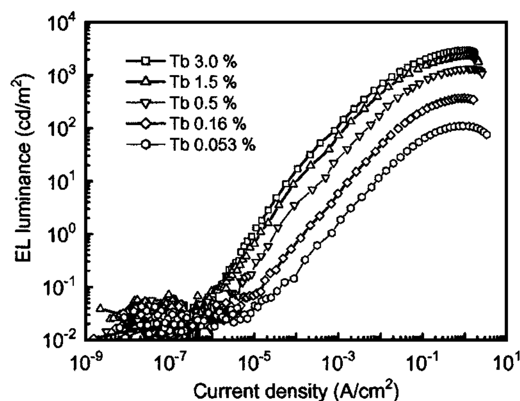

FIG. 6. EL luminance vs the injection current density for samples containing different Tb concentrations from 0.05% to 3%. All samples were annealed at 800 °C for 1 h.

Figure 6 shows the dependence of the EL luminance on the current density for five samples containing different Tb concentrations from 0.05% to 3% after annealing at 800 °C for 1 h. Initially the EL intensity has a linear relationship with injection current density, and then it saturates at high current density with a maximum intensity limited by the Tb concentration. A high luminance of up to 2800 cd/m^2 is achieved for a Tb concentration of 3%. Figure 7 illustrates the dependencies of the EL power efficiency and the external quantum efficiency on the Tb concentration for samples annealed at 800 and 900 °C. A decrease of the EL efficiency is observed at the higher annealing temperature of 900 °C for samples with a Tb concentration above 0.5%. The EL efficiency increases linearly with increasing the Tb concentra-

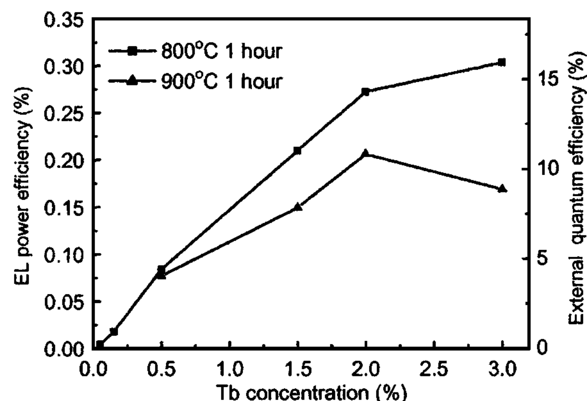

FIG. 7. Dependencies of the EL power efficiency and the external quantum efficiency on the Tb concentration at a current of 10 μA for a device size of 0.5 mm in diameter. The samples were annealed at 800 and 900 °C.

Downloaded 21 Jun 2005 to 134.34.145.184. Redistribution subject to AIP license or copyright, see http://jap.aip.org/jap/copyright.jsp

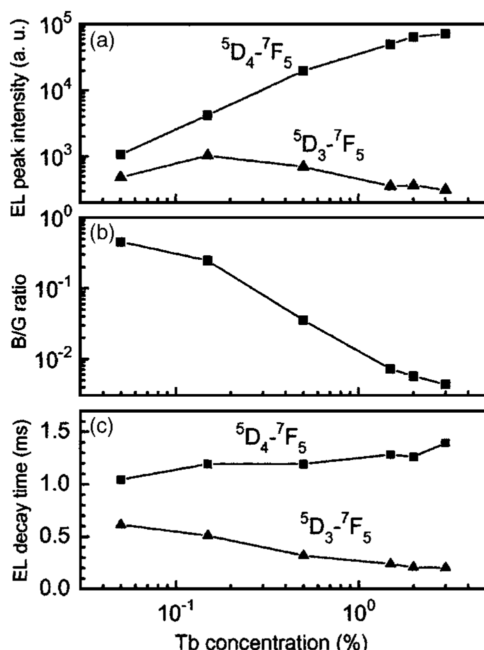

FIG. 8. Concentration dependencies of the EL intensity (a), the blue/green ratio (B/G ratio) (b), and the lifetime (c) of the two transitions from $^5D_3$ to $^7F_5$ (blue peak at 413 nm) and $^5D_4$ to $^7F_5$ (green peak at 541 nm). The samples were annealed at 800 °C for 1 h. The EL intensity was measured at a constant current injection of 10 μA.

tion and then saturates above 2% due to the concentration quenching effect (see below). A high power efficiency of 0.3% (corresponding to an external quantum efficiency of 16% and luminous efficiency of 2.1 lm/W) is obtained for the devices with a Tb concentration of 3%. (The scaling factor between external quantum efficiency and power efficiency is $eV/\hbar\omega$, where V is the operating voltage and $\hbar\omega$ is the emission photon energy.) The quantum efficiency of our devices is comparable to those of InGaN quantum well green light-emitting diodes (16.5%).[19]

B. Tb concentration

Figure 8(a) compares the concentration dependence of the EL peak intensity of the $^5D_3$–$^7F_5$ (blue peak at 413 nm) and $^5D_4$–$^7F_5$ (green peak at 541 nm) transitions for the samples annealed at 800 °C for 1 h. The EL intensity is measured at a constant current injection of 10 μA. The green peak increases linearly with increasing the Tb concentration up to 2% and then saturates, while the blue peak shows a strong concentration quenching after increasing the Tb concentration above 0.15%. Figure 8(b) shows the peak intensity ratio of the blue divided by the green peak (B/G ratio) as a function of the Tb concentration. The B/G ratio decreases with increasing Tb concentration, which indicates a more effective population of the $^5D_4$ levels. To trace back the origin of this behavior, we have measured the EL decay time of the blue ($^5D_3$) and green ($^5D_4$) lines [Fig. 8(c)]. The decay time of the $^5D_3$ level decreases with increasing Tb concentration, while the decay time of the $^5D_4$ level slightly increases. This indicates a faster nonradiative decay of $^5D_3$, leading to a higher average population of $^5D_4$. We ascribe this behavior to the crossrelaxation from the $^5D_3$ to the $^5D_4$ level in adjacent Tb^{3+} ions, made possible through the very small energy mismatch of 11 meV for ($^5D_3$–$^5D_4$) $\cong$($^7F_0$–$^7F_6$), as shown in the diagram of Fig. 9. A similar effect has been previously observed in Tb-doped yttrium silicate glass.[20] As a result the relative intensity of the green emission increases for higher Tb concentration.

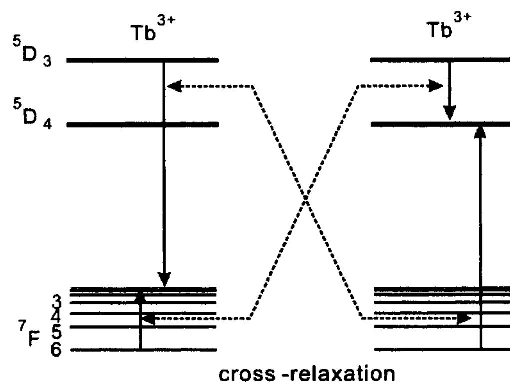

FIG. 9. Schematic crossrelaxation from $^5D_3$ to $^5D_4$ level of Tb^{3+} ions. It causes a quenching of the $^5D_3$ levels and a simultaneous enhancement for the excitation of the $^5D_4$ levels at high Tb concentration.

C. Annealing temperature

The annealing temperature dependencies of the blue (413 nm) and the green (541 nm) peaks were studied on samples with a constant Tb concentration of 1.5%. All EL spectra were again measured at a constant current injection of 10 μA. Upon increasing the annealing temperature from 800 to 1100 °C, the EL intensity of both peaks strongly decreases, while the B/G ratio increases in the EL spectra, as shown in Figs. 10(a) and 10(b). Since the lifetime of the green peak stays nearly constant and the lifetime of the blue

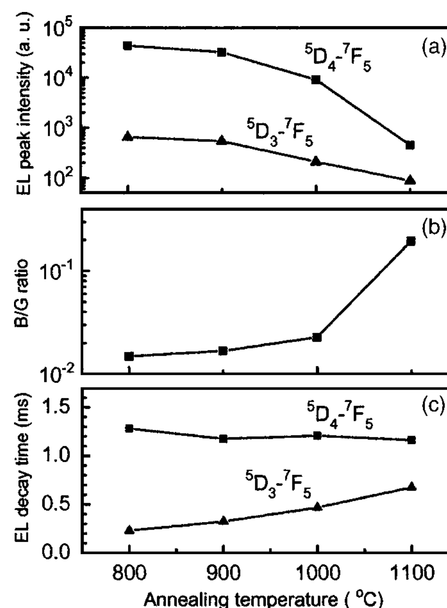

FIG. 10. Annealing temperature dependencies of the EL intensity (a), the blue/green ratio (b), and the lifetime (c) of the two transitions from $^5D_3$ to $^7F_5$ (413-nm blue peak) and $^5D_4$ to $^7F_5$ (541-nm green peak) for the samples. The Tb concentration is constant at 1.5% for all samples; and the injection current is 10 μA.

Downloaded 21 Jun 2005 to 134.34.145.184. Redistribution subject to AIP license or copyright, see http://jap.aip.org/jap/copyright.jsp

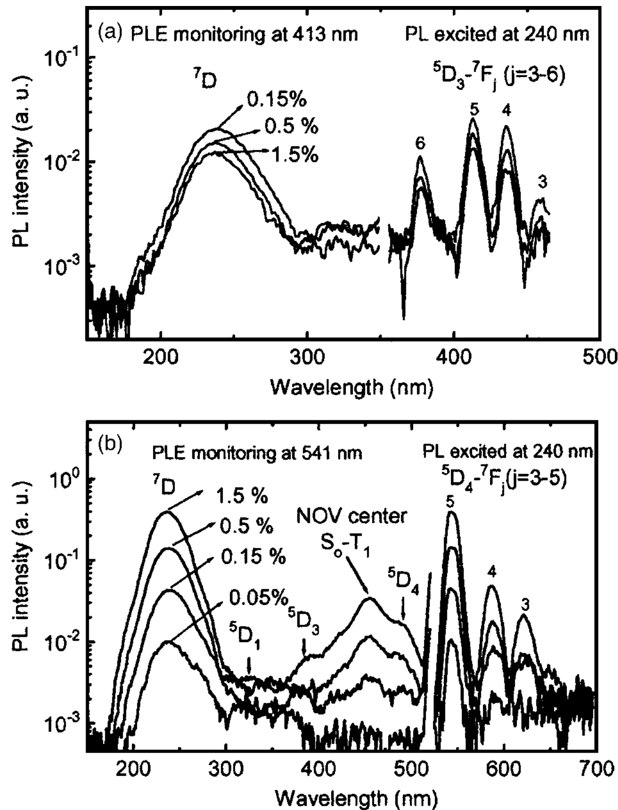

FIG. 11. PL spectra of the electronic transitions from $^5D_3$ to ^7F_j (j=3–6) (a) and from $^5D_4$ to ^7F_j (j=3–5) (b), excited with 240-nm radiation. In addition the PLE spectra are shown, detected at 413 (a) and 541 nm (b), respectively. The excitation goes from the $^7F_6$ ground state to different excited levels, as indicated in the figures. The excitation of the $S_0 \rightarrow T_1$ transition of the neutral oxygen vacancy (NOV) (≡Si–Si≡) centers in SiO_2 is also marked in (b).

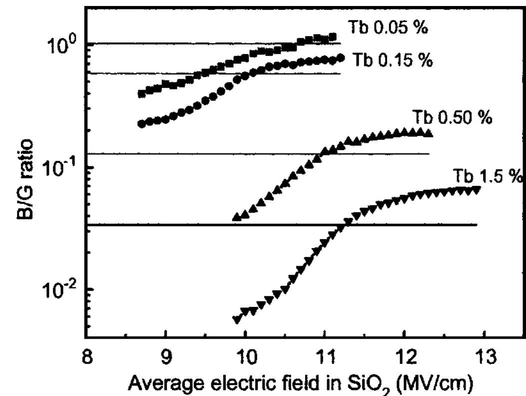

FIG. 12. Dependence of the blue/green ratio of the EL spectra on the average electric field for samples with different Tb concentrations of 0.05%, 0.15%, 0.5%, and 1.5%. The horizontal lines show the values of the B/G ratio of the PL spectra under the excitation by UV light with a photon energy of 5.16 eV (240 nm).

peak even shows an increase with increasing annealing temperature in Fig. 10(c), the decrease of the EL intensity cannot result from a faster nonradiative decay. Instead it has to come from a reduction of the number of effective Tb^{3+} luminescent centers. This is probably due to the formation of optically inactive Tb clusters at a high annealing temperature, which is similar to clustering of Er atoms in Er-implanted SiO_2.[21]

D. Excitation mechanism

Figures 11(a) and 11(b) show the PL and PLE spectra of the electronic transitions from the two excited energy levels $^5D_3$ and $^5D_4$, respectively. The PLE spectra in Figs. 11(a) and 11(b) were measured by monitoring the blue peak from $^5D_3$ to $^7F_5$ and the green peak from the $^5D_4$ to $^7F_5$ transition, the PL spectra were measured by 240-nm (5.16-eV) UV excitation. Similar to the EL results, comparable concentration dependencies of the green and blue peaks were observed in the PL spectra. Both peaks have an excitation peak at 240 nm, which is observed in many silicate phosphors such as Tb^{3+}-doped Y_2SiO_5 (Ref. 20) and YSiAlON glasses.[22] This excitation peak has ascribed to the ^7D level of Tb^{3+} respectively. The different excitation peaks at around 300–380 nm may come from the excitation from the ground-state $^7F_6$ to several close energy levels, $^5D_1$, $^5D_2$, $^5L_9$, $^5L_{10}$, and $^5D_3$ of the Tb^{3+} ions.[17,22] The excitation peak at 455 nm is absent in the excitation spectra of other Tb^{3+}-doped silicate phosphors. Probably it results from the energy transfer of the excitation $S_0 \rightarrow T_1$ of the neutral oxygen vacancy (NOV) (≡Si–Si≡) centers in SiO_2 created by ion implantation, which has a similar transition energy at around 2.65 eV (470 nm).[23] The peak at 490 nm can be attributed to the excitation of electrons from the $^7F_6$ to the $^5D_4$ level.

The EL from rare-earth ions embedded in a matrix under high electric field can be excited via two processes. One is the direct impact excitation of the rare-earth ion by energetic hot electrons in the conduction band of the matrix. The charge states of the rare-earth ions do not change during the excitation process. The other process is the excitation across the host band gap or of defects, and subsequent energy transfer to the rare-earth ions. In the former process, the relative intensity of the peaks from higher excited levels normally increases faster with increasing electric field than those at lower energy levels due to an increase of the average energy of the hot electrons. This phenomenon was observed in ZnS:Er and ZnS:Tb thin-film EL devices.[24,25] In the latter process, since the excitation comes from the energy transfer, the relative intensity of the emission peaks of rare-earth ions is mainly controlled by the thermal equilibrium between different energy levels of the rare-earth ions. Therefore, the relative intensity of the different peaks will not change dramatically with increasing electric field. Examples are ZnS:Tm or CaS:Tm thin-film EL devices.[26]

In order to check the probable EL excitation process in the SiO_2:Tb MOS devices, the B/G ratio of the EL spectra is plotted versus the average electric field in Fig. 12 for samples with different Tb concentrations. An increase of the B/G ratio of the EL spectra (prior to the saturation of excitation) was observed with increasing electric field. This gives strong evidence that the EL excitation is dominated by direct impact excitation from FN tunneling injection of hot electrons into the conduction band of SiO_2, as shown in Fig. 5. The strong decrease of the B/G ratio with increasing Tb concentration shows that the crossrelaxation from the higher excitation level $^5D_3$–$^5D_4$ is also involved in the excitation of

Downloaded 21 Jun 2005 to 134.34.145.184. Redistribution subject to AIP license or copyright, see http://jap.aip.org/jap/copyright.jsp

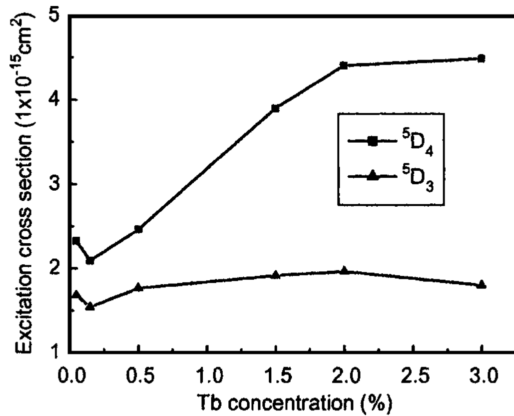

FIG. 13. Calculated EL excitation cross sections of the $^5D_3$ and $^5D_4$ levels as a function of the Tb concentration.

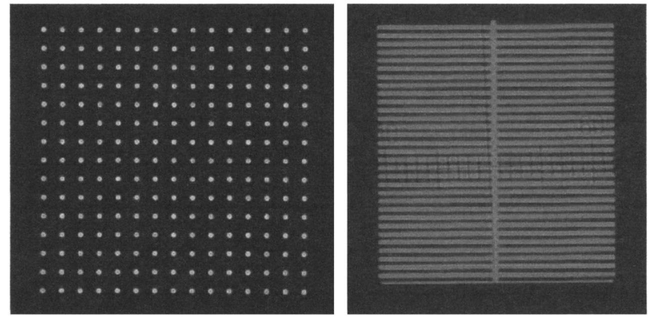

FIG. 14. (Color online) (a) Photograph of an array of 15×15 Tb-doped SiO_2 MOS light-emitting devices with a diameter of 20 μm and a space of 70 μm under an optical microscope; each of the devices is driven by a current of 0.2 μA. (b) Photograph of a comblike MOS light-emitting device with a stripe width of 4 μm taken under an injection current of 10 μA.

the lower-lying $^5D_4$ level. Therefore, the peaks of $^5D_4-^7F_j$ ($j=3-6$) transitions were excited by both the impact excitation and the crossrelaxation from $^5D_3$ states at high Tb concentration. The above excitation mechanism explains the change of EL spectra with Tb concentration and annealing temperature in Tb-doped SiO_2 MOS devices. It also explains the correlation between the onset of the EL and the strong FN tunneling injection of hot electrons as shown in Fig. 4.

E. EL excitation cross section

If the excitation process is dominated by the direct impact excitation, the change of the B/G ratio of the Tb^{3+} luminescence may reflect an increase of the average energy of hot electron with increasing the electric field. The hot electrons for EL excitation may have an equivalent average energy similar to the PL excitation photon energy for the EL spectra with the same B/G ratio compared to the PL spectra. The B/G ratio of the PL spectra under excitation of photon energy of 5.16 eV (240 nm) is also marked by the horizontal lines for different Tb concentrations in Fig. 12. The intersections indicate that the average hot electrons may have an equivalent average energy around 5.16 eV at an electric field around 10–11 MV/cm. This value is consistent with the average hot electron energy determined at the same electric field in SiO_2 by different techniques such as vacuum emission, carrier separation, and EL.[27]

The dependence of the EL intensity, I_{EL}, on the charge flux, J/e, can be simulated by the equation

$$I_{EL} = I_{max}\frac{J/e}{J/e + 1/\sigma\tau},$$

where I_{max}, σ, and τ are the saturated EL intensity, the excitation cross section, and the total lifetime of an excited level, respectively. The product of $\sigma\tau$ can be evaluated by fitting the dependence of I_{EL} vs J/e for the blue and green peaks from the $^5D_3$ and the $^5D_4$ levels. Figure 13 is the calculated EL excitation cross sections of the $^5D_3$ and the $^5D_4$ levels as a function of the Tb concentration. The excitation cross section of the $^5D_4$ level strongly increases from 2.1 to 4.4 $\times10^{-15}$ cm^2 with increasing Tb^{3+} concentration from 0.15% to 2%, whereas the cross section of the $^5D_3$ level stays nearly constant. This can again be interpreted by the crossrelaxation from the $^5D_3$ to $^5D_4$ level with increasing Tb concentration.

F. Device geometry

Small devices are usually needed for the integration of MOS light emitters on silicon chips for different applications. Therefore, various shapes of MOS devices with different feature sizes in the range of 2–500 μm were fabricated for testing the operation of the EL devices in dependence on the geometry. Figure 14(a) shows a photograph of an array of 15×15 MOS light-emitting devices with a diameter of 20 μm and a distance of 70 μm, which was taken under an optical microscope by a normal digital camera. Each of the devices was driven by a small current of 0.2 μA. Figure 14(b) shows a photograph of a comblike MOS light-emitting devices with a stripe width of 4 μm. The smallest fabricated MOS light-emitting device had a diameter of 2 μm, only limited by the optical lithography system available to us. The green light emission under the microscope was well visible with the bare eye at an injection current of a few nanoamperes. This demonstrates that the MOS light-emitting devices with a feature size in the (sub)micrometer range could be directly integrated on ULSI circuits or lab-on-a-chip systems.

IV. SUMMARY

In summary, efficient green electroluminescence was obtained from indium-tin-oxide/SiO_2:Tb/Si MOS devices doped by Tb^+ implantation. The EL efficiency increases linearly with increasing the implantation doses for a Tb concentration below 2%. The optimized device shows high external quantum efficiency above 16% and a luminous efficiency of 2.1 lm/W. The excitation of the EL can be attributed to the direct impact excitation of the Tb^{3+} ions by hot electrons with an impact excitation cross section up to 4.4 $\times10^{-15}$ cm^2. The crossrelaxation from the higher excited levels to the lowest excited levels of Tb^{3+} restricts the concentration quenching of the green luminescence peaks, which enables the fabrication of efficient green EL devices at a high Tb concentration. Light-emitting devices with a micrometer feature size were demonstrated by the metal-oxide-semiconductor technology.

Downloaded 21 Jun 2005 to 134.34.145.184. Redistribution subject to AIP license or copyright, see http://jap.aip.org/jap/copyright.jsp

ACKNOWLEDGMENTS

The authors would like to thank J. Winkler and F. Ludewig for the ion implantation, and H. Felsmann, C. Neisser, and G. Schnabel for the processing of the MOS structures.

[1]L. Pavesi, J. Phys.: Condens. Matter **15**, R1169 (2003).
[2]K. D. Hirschman, L. Tsybeskov, S. P. Duttagupta, and P. M. Fauchet, Nature (London) **384**, 338 (1996).
[3]G. T. Reed and A. P. Knights, *Silicon Photonics: An Introduction* (Wiley, New York, 2004).
[4]M. Salib, L. Liao, R. Jones, M. Morse, A. Liu, D. Samara-Rubio, D. Alduino, and M. Paniccia, Intel Technol. J. **8**, 142 (2004).
[5]Y. Kunemitsu, Phys. Rep. **263**, 1 (1995).
[6]L. Pavesi, L. Dal Negro, C. Mazzoleni, G. Franzò, and F. Priolo, Nature (London) **408**, 440 (2000).
[7]M. A. Green, J. Zhao, A. Wang, P. J. Reece, and M. Gal, Nature (London) **412**, 805 (2001).
[8]J. M. Sun, T. Dekorsy, W. Skorupa, B. Schmidt, and M. Helm, Appl. Phys. Lett. **83**, 3385 (2003).
[9]L. Rebohle, J. von Borany, D. Borchert, H. Fröb, T. Gebel, M. Helm, W. Möller, and W. Skorupa, Electrochem. Solid-State Lett. **4**, G57 (2001).
[10]F. Iacona *et al.*, Appl. Phys. Lett. **81**, 3242 (2002).
[11]A. Nazarov, J. M. Sun, I. N. Osiyuk, I. P. Tjagulskii, V. S. Lysenko, W. Skorupa, R. A. Yankov, and T. Gebel, Appl. Phys. Lett. (in press).
[12]M. E. Castagna, S. Coffa, M. Monaco, A. Muscara, L. Caristia, S. Lorenti, and A. Messina, Mater. Sci. Eng., B **105**, 83 (2003).
[13]S. Y. Seo, J. H. Shin, B. S. Bae, N. Park, J. J. Penninkhof, and A. Polman, Appl. Phys. Lett. **82**, 3345 (2003).
[14]M. Yoshihara, A. Sekiya, T. Morita, K. Ishii, S. Shimoto, S. Sakai, and Y. Ohki, J. Phys. D **30**, 1908 (1997).
[15]H. Amekura, A. Eckau, R. Carius, and Ch. Buchal, J. Appl. Phys. **84**, 3867 (1998).
[16]J. M. Sun, W. Skorupa, T. Dekorsy, M. Helm, L. Rebohle, and T. Gebel, Appl. Phys. Lett. **85**, 3387 (2004).
[17]G. H. Dieke, *Spectra and Energy Levels of Rare Earth Ions* (Interscience, New York, 1969).
[18]J. A. Lopez-Villanueva, J. A. Jimenez-Tejada, P. Cartujo, J. Bausells, and J. E. Carceller, J. Appl. Phys. **70**, 3712 (1991).
[19]S. Nagahama *et al.*, Phys. Status Solidi A **188**, 1 (2001).
[20]Y. Y. Choi, K.-S. Sohn, H. D. Park, and S. Y. Choi, J. Mater. Res. **16**, 881 (2001).
[21]A. Polman, J. Appl. Phys. **82**, 1 (1997).
[22]D. de Graaf, *Chemistry, Structure and Properties of Rare-Earth Containing Si-Al-O-N Glasses*, Ph.D thesis, Technische Universiteit Eindhoven, The Netherlands, 2004, p. 68.
[23]L. Rebohle, J. von Borany, H. Fröb, and W. Skorupa, Appl. Phys. B: Lasers Opt. **70**, 1 (2000).
[24]L. Ma, G. Zhong, and S. Xu, Chinese Lumin. Display 6, 192 (1985).
[25]D. C. Krupka, J. Appl. Phys. **43**, 476 (1972).
[26]J. M. Sun, G. Z. Zhong, X. W. Fan, C. W. Zheng, G. O. Mueller, and R. Mueller-Mach, J. Appl. Phys. **83**, 3374 (1998).
[27]D. J. DiMaria, E. Cartier, and D. Arnold, J. Appl. Phys. **73**, 3367 (1993).

Downloaded 21 Jun 2005 to 134.34.145.184. Redistribution subject to AIP license or copyright, see http://jap.aip.org/jap/copyright.jsp